SUPPLEMENTARY INFORMATION

The Effect of Water on Gold Supported Chiral Graphene Nanoribbons: Rupture of Conjugation by an Alternating Hydrogenation Pattern

Alejandro Berdonces-Layunta,[ab‡*] Adam Matěj,[cde‡*] Alejandro Jiménez-Martín,[cdf] James Lawrence,[ab] Mohammed S. G. Mohammed,[ab] Tao Wang,[ab] Benjamin Mallada,[cde] Bruno de la Torre,[d] Adrián Martínez,[g] Manuel Vilas-Varela,[g] Reed Nieman,[h] Hans Lischka,[h] Dana Nachtigallová,[ij] Diego Peña,[g] Pavel Jelínek,[cd*] Dimas G. de Oteyza[abk*]

a Donostia International Physics Center, 20018 San Sebastián, Spain

b Centro de F´ısica de Materiales, 20018 San Sebastián, Spain

c Institute of Physics, Czech Academy of Sciences, 16200 Prague, Czech Republic

d Regional Centre of Advanced Technologies and Materials, Czech Advanced Technology and Research Institute (CATRIN), Palack´y University,783 71 Olomouc, Czech Republic

e Department of Physical Chemistry, Faculty of Science, Palack´y University, 779 00 Olomouc, Czech Republic

f Faculty of Nuclear Sciences and Physical Engineering, Czech Technical University in Prague, Brehova 7, Prague 1 115 19, Czech Republic

g Centro Singular de Investigación en Química Biolóxica e Materiais Moleculares (CiQUS), and Departamento de Química Orgánica, Universidade de Santiago de Compostela, 15705 Santiago de Compostela, Spain

h Department of Chemistry and Biochemistry, Texas Tech University, Lubbock, TX 79409-1061, USA

i Institute of Organic Chemistry and Biochemistry, Czech Academy of Sciences, 16000

j IT4Innovations, VSB-Technical University of Ostrava, 17. Listopadu 2172/15, Ostrava-Poruba 70800, Czech Republic

k Nanomaterials and Nanotechnology Research Center (CINN), CSIC-UNIOVI-PA, 33940 El Entrego, Spain

Methods

The Au(111) surface (MaTeck) was prepared by standard sputtering and annealing cycles. The precursor of the ribbons, 10,10’-dibromo-9,9’-bianthracene (DBBA),[1] was deposited via thermal evaporation at 160 °C onto the substrate while it was held at room temperature. To form the nanoribbons, the substrate was then annealed via radiative heating to 320 °C for 30 min. For the exposure we used a homebuilt gas line attached to a leak valve. The liquid was introduced in a glass ampoule connected to the system and heated to its boiling temperature in order to increase its vapor pressure. Successive purging cycles were performed prior to the actual sample exposure. Multiple samples were prepared with different exposure conditions. In the case of water, they ranged from 2E-7 mbar for 1 hour to 8E-7mbar for 2.5 hours, whereas for the ethanol experiment we employed 7E-8 mbar for 20 minutes. The purity of the atmosphere was checked by means of a mass spectrometer during the process.

All SPM experiments were performed using a commercial Scienta-Omicron LT-STM/AFM, cooled to 4.3 K. CO was then deposited onto the sample via a leak valve at a pressure of approximately 5×10^{-9} mbar for a total time of 60 s and a maximum sample temperature of 7.0 K. CO was picked up with the tip by scanning at constant current, with typical feedback parameters at negative sample bias values around -500 mV and 1 nA until a sudden improvement in the resolution happened. dI/dV experiments were typically performed using a digital lock-in, with an oscillation frequency of 731 Hz and an amplitude of 5-20 mV. Images were analyzed with the freeware program WSxM.[2]

Quantum mechanical calculations were carried out using Gaussian16[3] program with longrange corrected hybrid functional ωB97X-D[4] with empirical dispersion, def2-SVP[5] basis set for water on gold calculations and cc-pVDZ[6] basis set for GNR calculations. Bond dissociation energy of water molecule was done in gas phase and adsorbed on gold, evaluated as energy difference between relaxed products and reactants. In the case of adsorbed water, the gold surface was modelled by 15 fixed gold atoms arranged into a cluster with lattice of fcc(111) surface and one gold adatom in HCP position, which was allowed to relax (see Supplementary figure 5). All gold atoms were calculated with pseudopotentials treating core electrons. Water molecule was then added to the adatom and relaxed. Both hydrogen and hydroxyl group as possible products were modelled adsorbed on the adatom and their binding energies compared. The relative energies in Figure 2 were obtained as difference of total energies of product and reactants, including the dissociation energy required to create two hydrogen radicals catalysed by Au adatom. Nucleus-independent chemical shifts were calculated using GIAO method[7] with dummy atoms placed 1 $^{\circ}$A above the center of each ring and only the zz components of shielding tensors were collected and their sign inversed, i.e, NICS(1)zz[8, 9] method (NICS used throughout text for simplicity). The results were plotted using circles proportional to the value over each ring with blue and red representing negative and positive magnetic shielding, respectively. The anisotropy of induced-current density was calculated only for π molecular orbitals, i.e, π-ACID (ACID used throughout text for simplicity), to focus on the conjugation of π electrons and the plots were rendered with isovalue 0.05 au.

Multireference average quadratic coupled cluster (MR-AQCC) calculations[10] were performed for the dimer and trimer structures using the 6-31G basis set.[11, 12, 13] Polarization functions were also utilized for the dimer structures with the 6-31G* basis set to show the basis set dependence.[14] A reference space consisting of six electrons in six orbitals (6,6) was used for

systems with even numbers of electrons, while seven electrons in six orbitals (7,6) was used for odd numbers of electrons. The orbitals for the MR-AQCC calculations were computed with the complete active space self-consistent field (CASSCF) theory.[15] For even numbers of electrons, a CAS(8,8) was used, while for odd numbers of electrons, a CAS(9,8) was used. All CASSCF and AQCC calculations were performed with symmetry restrictions and the CS point group. The A' irreducible representation contained all the σ orbitals for the pristine structures without any additional hydrogen, so these orbitals were kept frozen at the SCF level in all cases. The π orbitals, present in the A" irreducible representation, were kept active. The A" component of the σ orbitals resulting from the formation of new C-H bonds were kept active as well. All MR-AQCC and CASSCF calculations were performed utilizing the COLUMBUS program package.[16, 17, 18]

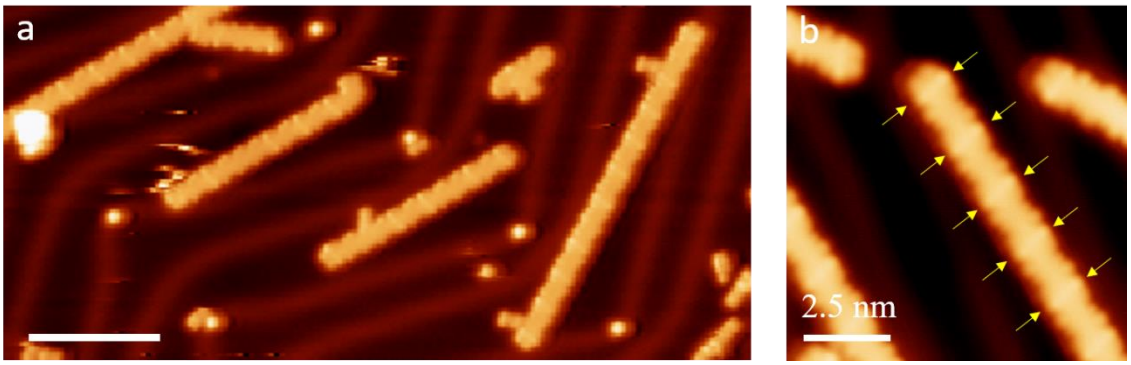

Figure 1: Sample exposed to 540 Langmuir of water. a)-1 V, 50 pA b)-1 V, 200 pA, metal tip.

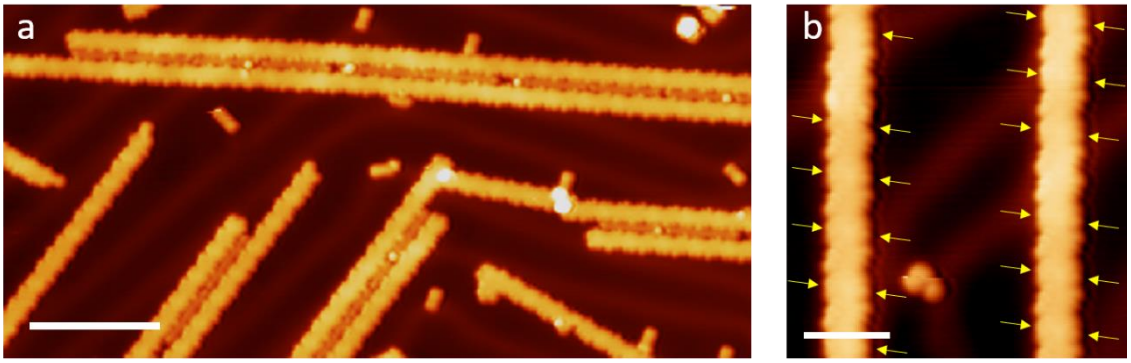

Figure 2: Sample exposed to 5400 Langmuir of water. a)-1V, 50 pA b)-1 V, 100 pA, CO tip. Hydrogenated segments are marked with yellow arrows. They can be identified by their straight appeareance.

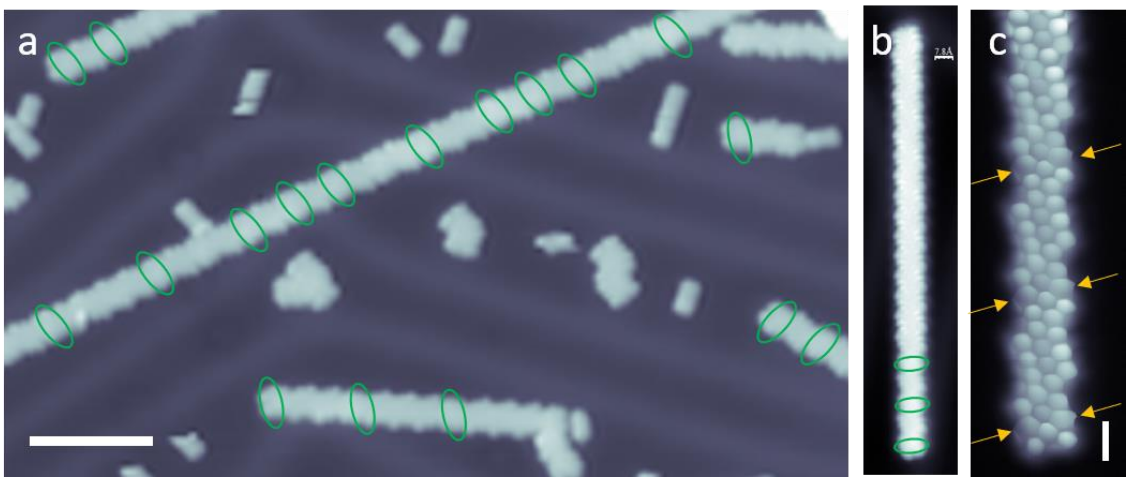

Figure 3: Sample exposed to EtOH. a) Survey of the sample, scale bar 5nm b) Ribbon with 3 unit cells hydrogenated c) Zoom in the ribbon defects, scale bar 5 Å.

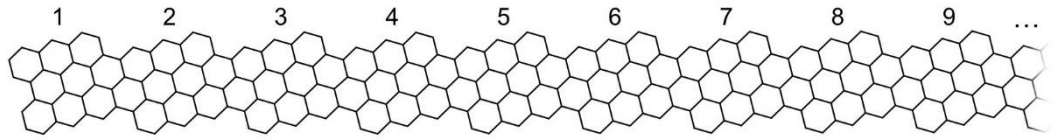

a

cell number	1	2	3	4	5	6	7	8	9	10	11	12	13	14	15	16	17	18	19	20
sample	82	82	80	75	70	54	46	31	20	14	12	8	7	5	3	2	2	2	2	2
hydrogenated	78	2	60	18	35	19	26	12	8	6	5	4	4	1	1	0	0	2	0	0
relative abundance	0.95	0.02	0.75	0.24	0.50	0.35	0.57	0.39	0.40	0.43	0.42	0.50	0.57	0.20	0.33	0.00	0.00	1.00	0.00	0.00

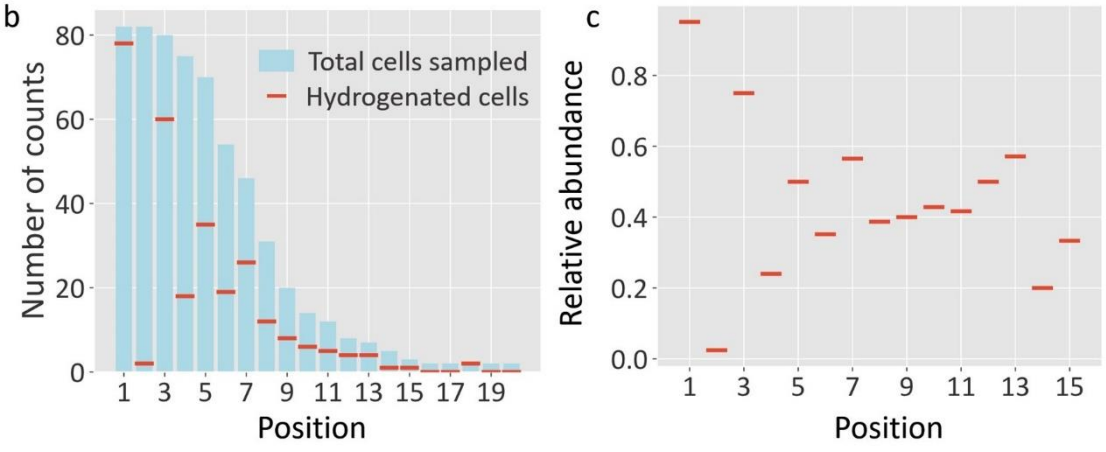

Figure 4: a) Statistics of the amount of hydrogenated cells by position on the ribbon. Position 1 refers to the terminal units, 2 to the second unit from the end and so on. b) plot of the data shown in a. c) Relative hydrogenation degree of the cells.

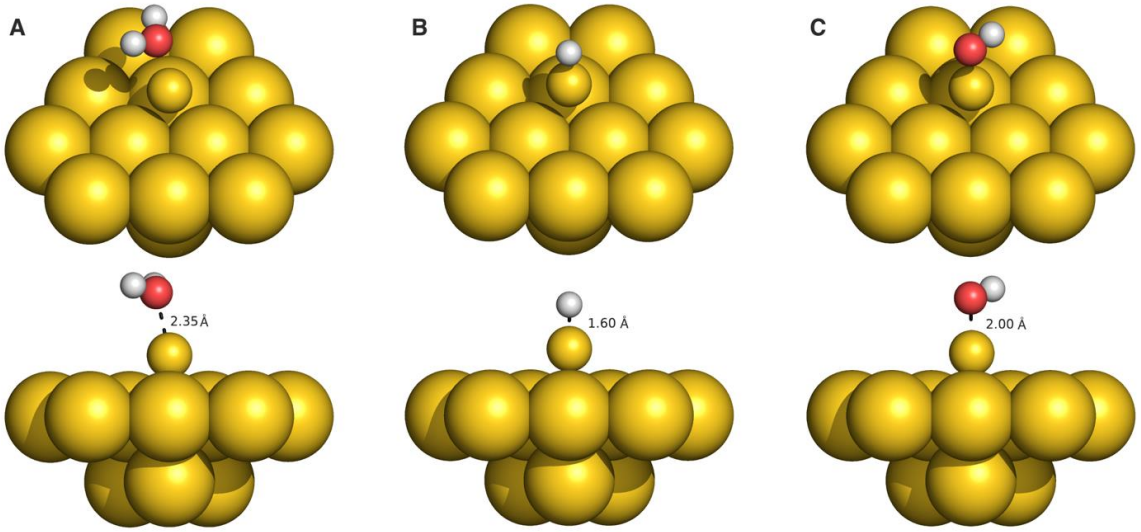

Figure 5: Relaxed structures of water molecule (a), hydrogen radical (b), and hydroxyl radical (c) adsorbed on gold adatom on fixed gold cluster.

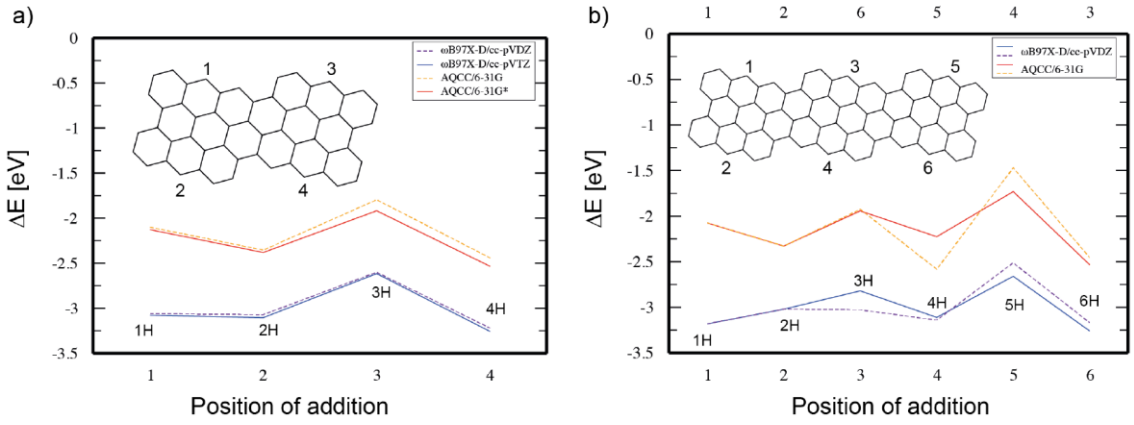

Figure 6: Comparison between DFT and MR-AQCC methods calculating relative energies of hydrogenation steps on dimer (a) and trimer (b), obtained as energy difference of products and reactants (energy of hydrogen radical included). Overlays illustrate positions of hydrogenation on the ribbons, numbering corresponds to x axes. Steps in panel (a) are consecutive, with 1-4 hydrogens added to dimer, resulting in fully hydrogenated ribbon. In panel (b), two sequences of hydrogenation are illustrated. Bottom x axis (solid lines) illustrates sequential hydrogenation, while top axis (dashed lines) illustrates hydrogenation of termini and subsequent hydrogenation of middle unit. Blue and violet curves represent DFT; red and orange stand for MR-AQCC method. For active spaces used in AQCC calculations see Methods.

		GNR length					
		2	3	4	5	6	7
DFT	HONO	1.63	1.57	1.54	1.53	1.52	1.52
	LUNO	0.37	0.43	0.46	0.47	0.48	0.48
	y_0	0.100	0.143	0.163	0.173	0.180	0.184
MR-AQCC	HONO	1.52	1.54				
	LUNO	0.48	0.47				
	y_0	0.181	0.170				

Table 1: Natural orbital occupation numbers and calculated diradical character with increasing length of GNR. For computational details see Methods.

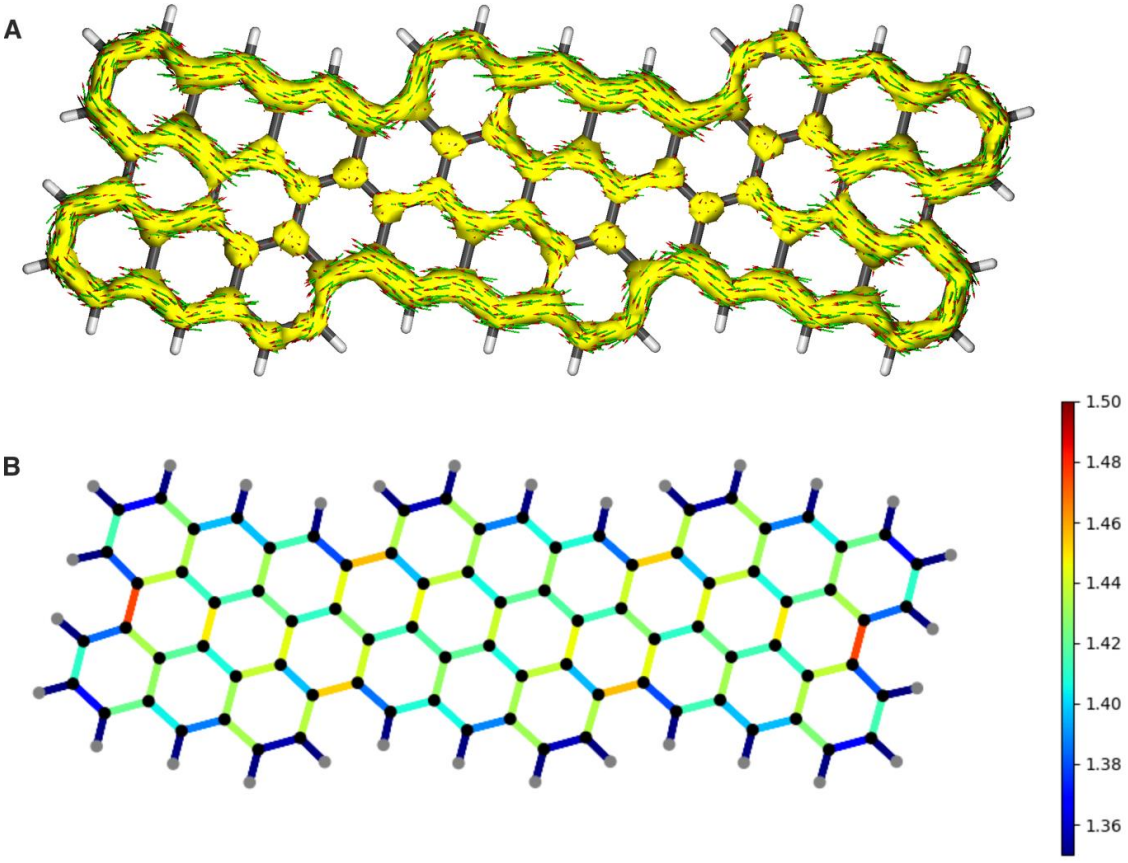

Figure 7: π -ACID plot of pristine GNR trimer (a), isovalue at 0.05 au, and bond length analysis (b).

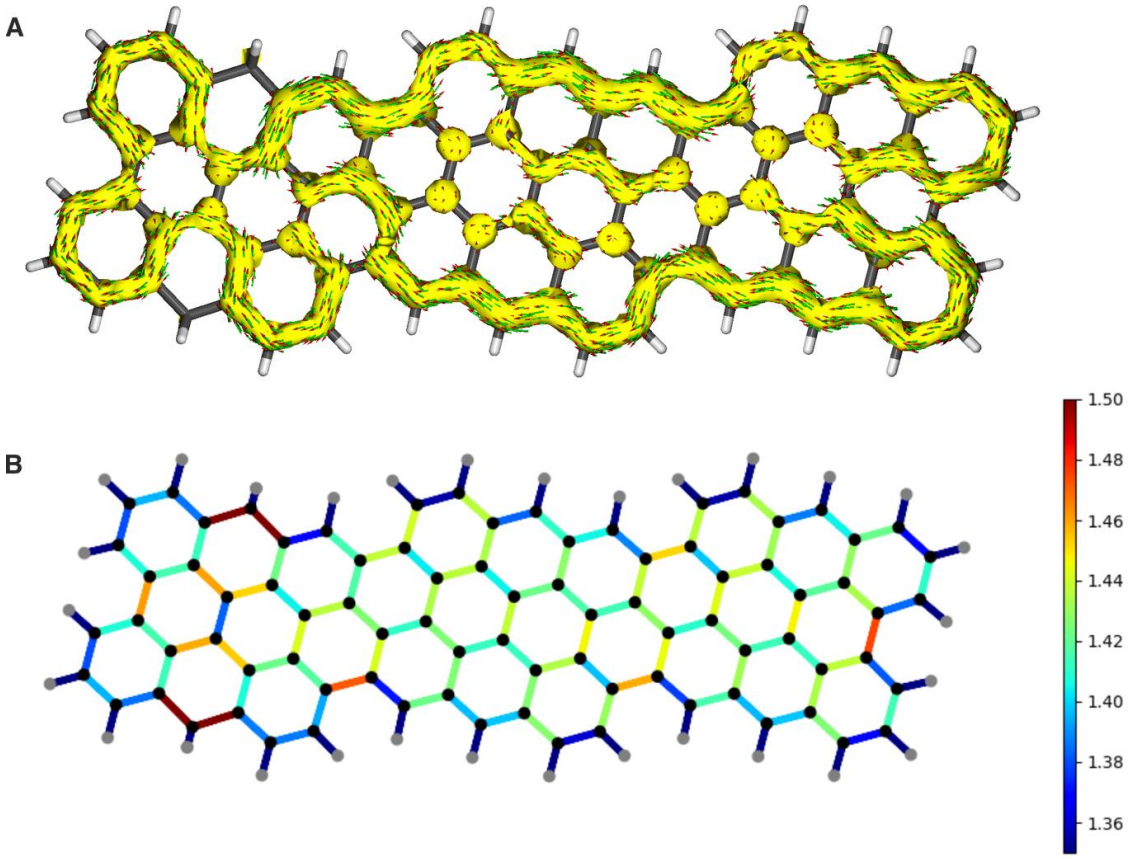

Figure 8: π -ACID of GNR with one terminal unit reduced (a), isovalue 0.05 au, and bond length análisis (b).

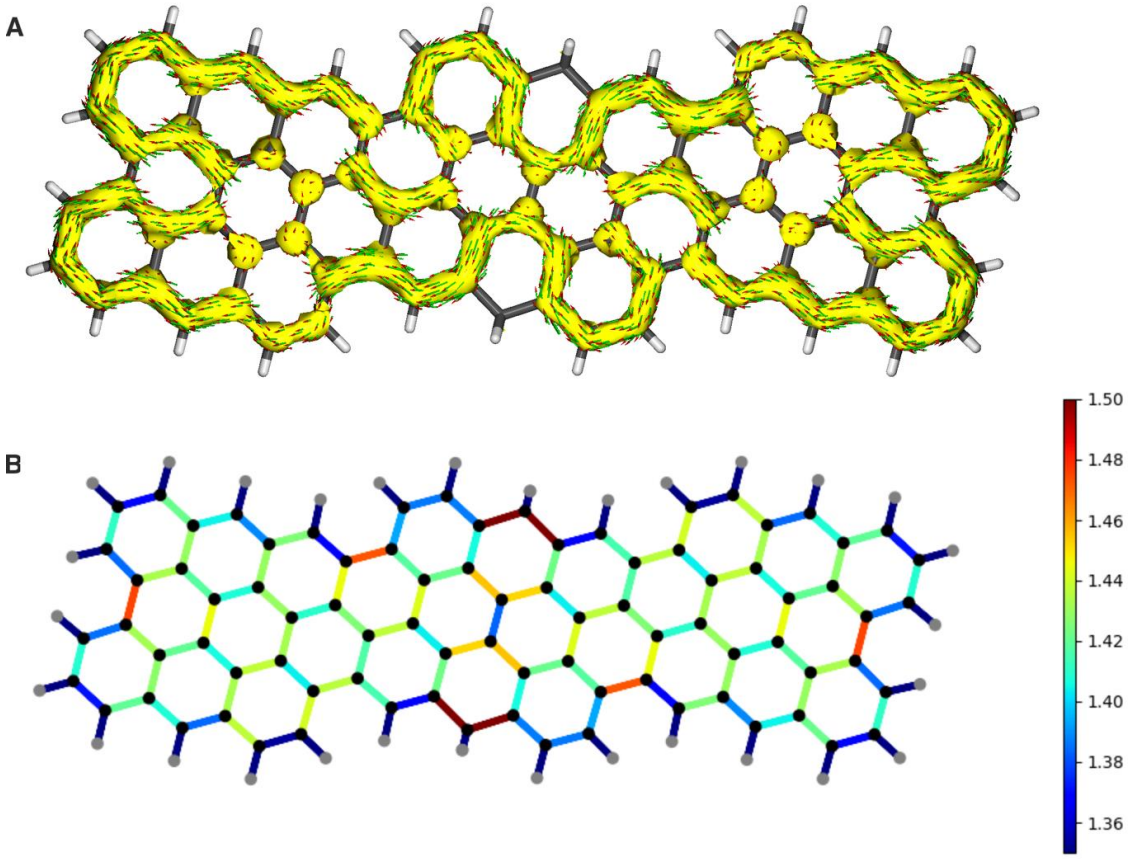

Figure 9: π -ACID of GNR with middle unit reduced (a), isovalue 0.05 au, and bond length analysis (b).

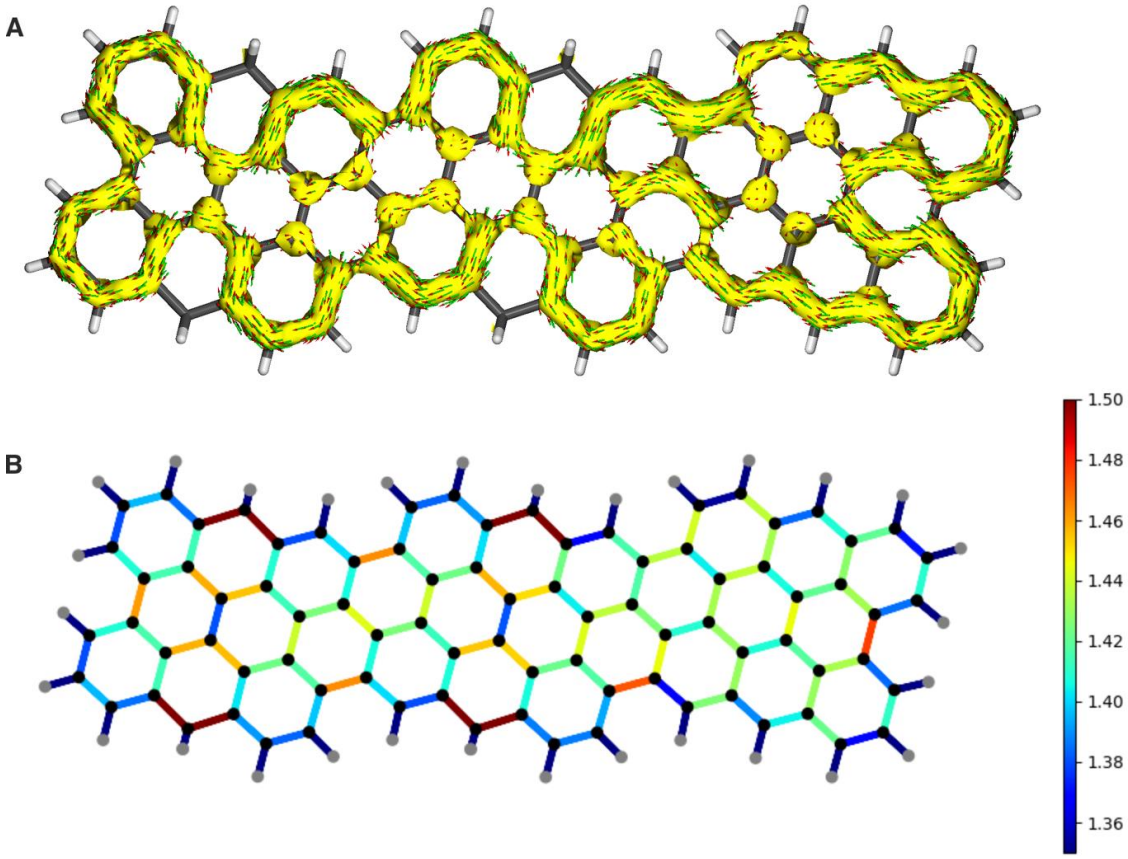

Figure 10: π -ACID of GNR with one terminal and middle units reduced (a), isovalue 0.05 au, and bond length analysis (b).

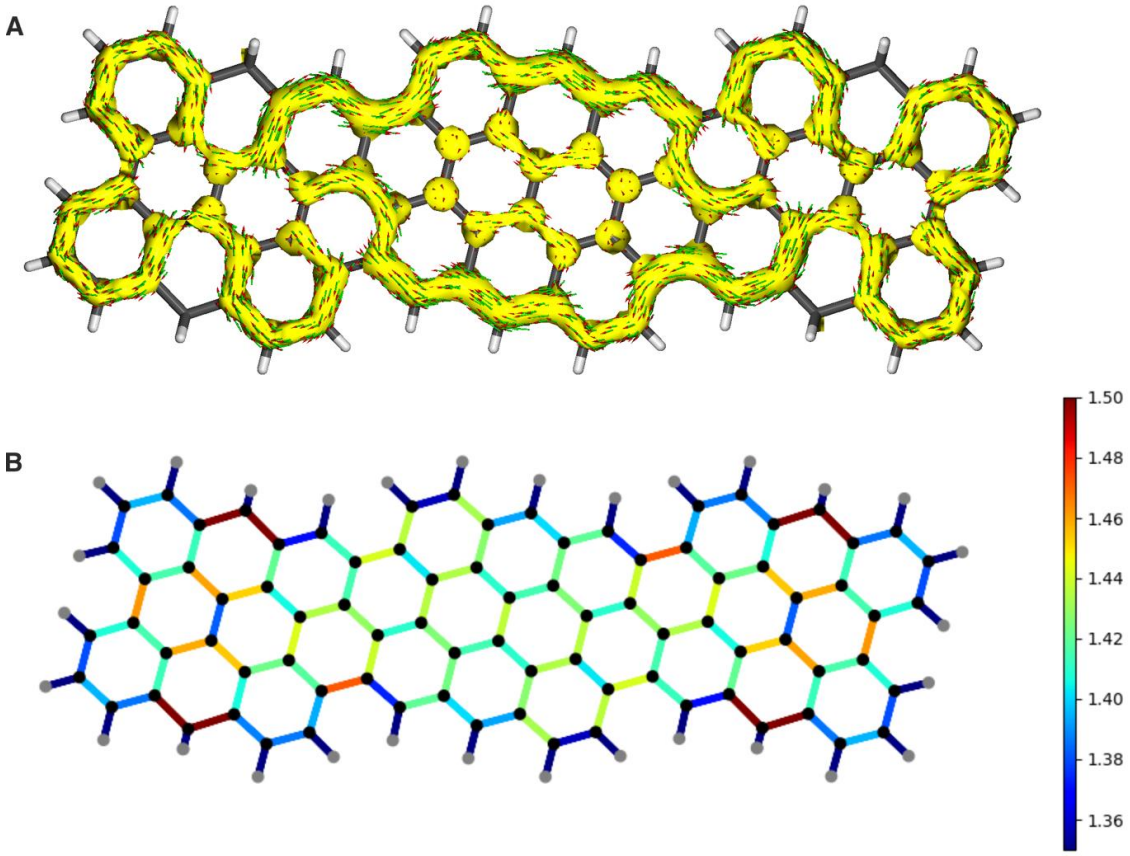

Figure 11: π -ACID of GNR with both terminal units reduced (a), isovalue 0.05 au, and bond length analysis (b).

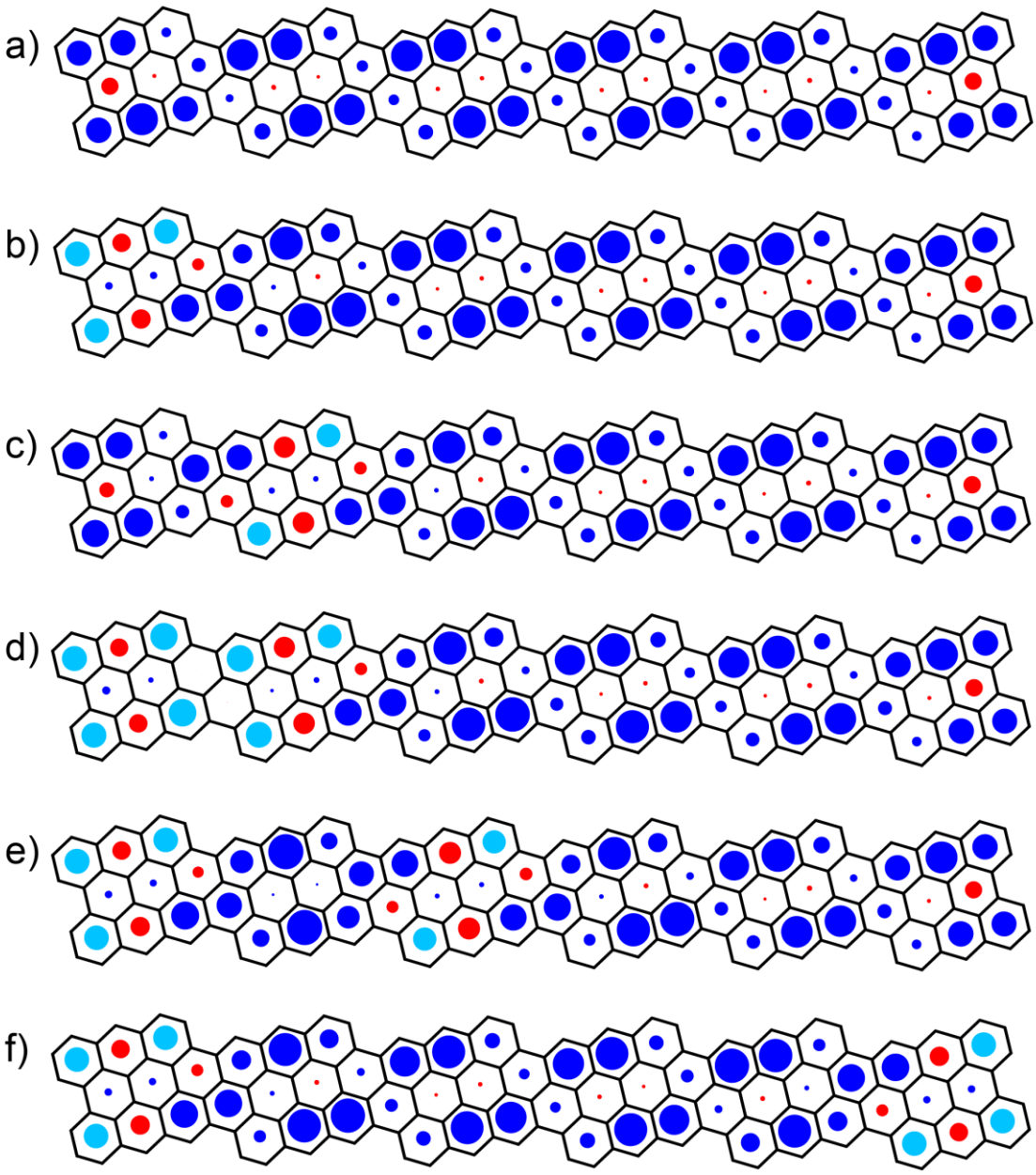

Figure 12: Plots of NICS(1)zz values for various GNRs. Diameters of circles are proportional to shielding values. Blue and red circles represent aromatic and antiaromatic rings, respectively. Light blue circles represent isolated benzene rings, i.e., Clar's sextets. (a) pristine GNR, (b) one terminal unit reduced, (c) second unit reduced, (d) first two units reduced, (e) first and third units reduced, (f) both terminal units reduced.

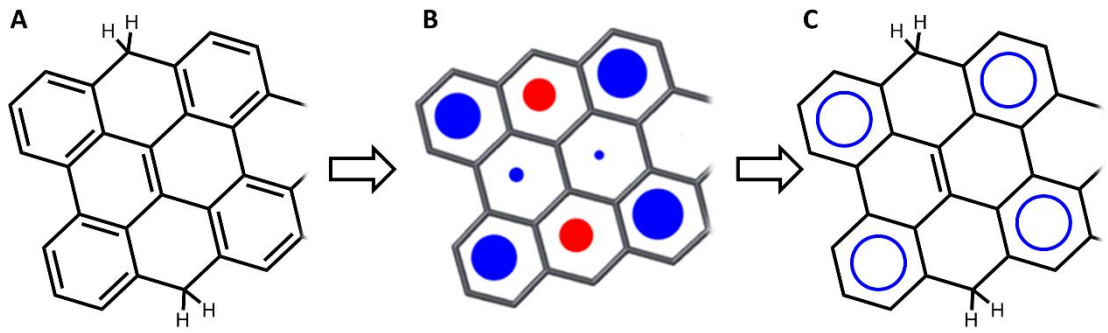

Figure 13: Some NICS or molecular structures suggest strongly localized aromatic character at specific rings. Those cases are close to the ideal example of Clar sextets. a) Detail of the molecular structure of an hydrogenated segment. b) NICS of the same region. c) Its Clar sextets distribution, as evidenced by both a) and b).

References

[1] D. G. de Oteyza, A. García-Lekue, M. Vilas-Varela, N. Merino-Díez, E. Carbonell-Sanromà, M. Corso, G. Vasseur, C. Rogero, E. Guitián, J. I. Pascual, J. E. Ortega, Y. Wakayama, and D. Peña, "Substrate-Independent Growth of Atomically Precise Chiral Graphene Nanoribbons," ACS Nano, vol. 10, no. 9, pp. 9000−9008, Sep. 2016. [Online]. Available: https://pubs.acs.org/doi/10.1021/acsnano.6b05269

[2] I. Horcas, R. Fernández, J. M. Gómez-Rodríguez, J. Colchero, J. Gómez-Herrero, and A. M. Baro, "WSXM</span : A software for scanning probe microscopy and a tool for nanotechnology," Review of Scientific Instruments, vol. 78, no. 1, p. 013705, Jan. 2007. [Online]. Available: http://aip.scitation.org/doi/10.1063/1.2432410

[3] M. J. Frisch, G. W. Trucks, H. B. Schlegel, G. E. Scuseria, M. A. Robb, J. R. Cheeseman, G. Scalmani, V. Barone, G. A. Petersson, H. Nakatsuji, X. Li, M. Caricato, A. V. Marenich, J. Bloino, B. G. Janesko, R. Gomperts, B. Mennucci, H. P. Hratchian, J. V. Ortiz, A. F. Izmaylov, J. L. Sonnenberg, D. Williams-Young, F. Ding, F. Lipparini, F. Egidi, J. Goings, B. Peng, A. Petrone, T. Henderson, D. Ranasinghe, V. G. Zakrzewski, J. Gao, N. Rega, G. Zheng, W. Liang, M. Hada, M. Ehara, K. Toyota, R. Fukuda, J. Hasegawa, M. Ishida, T. Nakajima, Y. Honda, O. Kitao, H. Nakai, T. Vreven, K. Throssell, J. A. M. Jr., J. E. Peralta, F. Ogliaro, M. J. Bearpark, J. J. Heyd, E. N. Brothers, K. N. Kudin, V. N. Staroverov, T. A. Keith, R. Kobayashi, J. Normand, K. Raghavachari, A. P. Rendell, J. C. Burant, S. S. Iyengar, J. Tomasi, M. Cossi, J. M. Millam, M. Klene, C. Adamo, R. Cammi, J. W. Ochterski, R. L. Martin, K. Morokuma, O. Farkas, J. B. Foresman, and D. J. Fox, "Gaussian16 Revision C.01," 2016, Gaussian Inc. Wallingford CT.

[4] J.-D. Chai and M. Head-Gordon, "Long-range corrected hybrid density functionals with damped atom−atom dispersion corrections," Physical Chemistry Chemical Physics, vol. 10, p. 6615, 2008.

[5] F. Weigend and R. Ahlrichs, "Balanced basis sets of split valence, triple zeta valence and quadruple zeta valence quality for H to Rn: Design and assessment of accuracy," Physical Chemistry Chemical Physics, vol. 7, pp. 3297−3305, 2005.

[6] T. H. Dunning, “Gaussian basis sets for use in correlated molecular calculations. I. The atoms boron through neon and hydrogen,” The Journal of Chemical Physics, vol. 90, pp. 1007–1023, 1989.

[7] R. Ditchfield, “Self-consistent perturbation theory of diamagnetism,” Molecular Physics, vol. 27, pp. 789–807, 4 1974.

[8] I. Cernusak, P. W. Fowler, and E. Steiner, “Ring currents in six-membered heterocycles: the diazaborinines (CH)2B2N2,” Molecular Physics, vol. 98, pp. 945–953, 7 2000.

[9] E. Steiner, P. W. Fowler, and L. W. Jenneskens, “Counter-rotating ring currents in coronene and corannulene,” Angewandte Chemie International Edition, vol. 40, pp. 362–366, 1 2001.

[10] P. G. Szalay and R. J. Bartlett, “Multi-reference averaged quadratic coupled-cluster method: a size-extensive modification of multi-reference CI,” Chemical Physics Letters, vol. 214, pp. 481–488, 11 1993.

[11] R. Ditchfield, W. J. Hehre, and J. A. Pople, “Self-consistent molecular-orbital methods. IX. An extended gaussian-type basis for molecular-orbital studies of organic molecules,” The Journal of Chemical Physics, vol. 54, pp. 724–728, 1 1971.

[12] G. A. Petersson, A. Bennett, T. G. Tensfeldt, M. A. Al-Laham, W. A. Shirley, and J. Mantzaris, “A complete basis set model chemistry. I. the total energies of closed-shell atoms and hydrides of the first-row elements,” The Journal of Chemical Physics, vol. 89, pp. 2193–2218, 8 1988.

[13] G. A. Petersson and M. A. Al-Laham, “A complete basis set model chemistry. II. open-shell systems and the total energies of the first-row atoms,” The Journal of Chemical Physics, vol. 94, pp. 6081–6090, 5 1991.

[14] W. J. Hehre, R. Ditchfield, and J. A. Pople, “Self–consistent molecular orbital methods. XII. Further extensions of gaussian–type basis sets for use in molecular orbital studies of organic molecules,” The Journal of Chemical Physics, vol. 56, pp. 2257–2261, 3 1972.

[15] B. O. Roos, P. R. Taylor, and P. E. Sigbahn, “A complete active space SCF method (CASSCF) using a density matrix formulated super-CI approach,” Chemical Physics, vol. 48, pp. 157–173, 5 1980.

[16] H. Lischka, T. Müller, P. G. Szalay, I. Shavitt, R. M. Pitzer, and R. Shepard, “Columbus–a program system for advanced multireference theory calculations,” WIREs Computational Molecular Science, vol. 1, pp. 191–199, 3 2011.

[17] H. Lischka, R. Shepard, T. Müller, P. G. Szalay, R. M. Pitzer, A. J. A. Aquino, M. M. A. do Nascimento, M. Barbatti, L. T. Belcher, J.-P. Blaudeau, I. Borges, S. R. Brozell, E. A. Carter, A. Das, G. Gidofalvi, L. González, W. L. Hase, G. Kedziora, M. Kertesz, F. Kossoski, F. B. C. Machado, S. Matsika, S. A. do Monte, D. Nachtigallov´a, R. Nieman, M. Oppel, C. A. Parish, F. Plasser, R. F. K. Spada, E. A. Stahlberg, E. Ventura, D. R. Yarkony, and Z. Zhang, “The generality of the guga mrci approach in columbus for treating complex quantum chemistry,” The Journal of Chemical Physics, vol. 152, p. 134110, 4 2020.

[18] H. Lischka, R. Shepard, I. Shavitt, R. M. Pitzer, T. M¨uller, P. G. Szalay, S. R. Brozell, G. Kedziora, E. A. Stahlberg, R. J. Harrison, J. Nieplocha, M. Minkoff, M. Barbatti, M. Schuurmann, Y. Guan, D. R. Yarkony, S. Mastika, F. Plasser, E. V. Beck, J.-P. Blaudeau, M. Ruckenbauer, B. Sellner, J. J. Szymczak, R. F. K. Spada, A. Das, L. T. Belcher, and R. Nieman, “COLUMBUS, an ab initio electronic structure program,” 2022, release 7.2.